All-Inorganic Colloidal Quantum Dot Photovoltaics Employing Solution-Phase Halide Passivation

*Zhijun Ning, Yuan Ren, Sjoerd Hoogland, Oleksandr Voznyy, Larissa Levina, Philipp Stadler, Xinzheng Lan, David Zhitomirsky, and Edward H. Sargent**

Colloidal quantum dots (CQDs) combine solution-phase synthesis and processing with attractive quantum-size-effect tuning. They have therefore seen intensive investigation in solar cells, photodetectors, and electroluminescent devices, each of which benefits from low cost, large area, and spectral tunability.[1–5]

Photovoltaics based on CQDs have seen particular emphasis since spectral tuning allows the bandgap of single-junction devices to be optimally matched to the solar spectrum, and further enables higher-efficiency tandem and multijunction solar cells, where quantum tuning alone provides the basis of bandgap customization within each junction.[6] Multi-exciton-generation devices are pursued with this same objective.[7]

Two key classes of advances had, until recently, dominated CQD photovoltaics (PV) progress. Short organic bidentate ligands, such as ethanedithiol and mercaptopropionic acid, were found to simultaneously passivate CQD surfaces and densify films within the solid state. Much effort has recently been invested in these solid-state ligand exchanges, which displace long insulating ligands such as oleic acid and replace them with short, strongly-bound, bifunctional ligands.[8–10] The second major performance-enhancing advance has been the realization of optimized device architectures, especially the depleted-heterojunction CQD solar cells. Here, a large-bandgap transparent electron-accepting n-type layer produces a depletion region in the p-type CQD solid, leading to efficient carrier extraction from a thickness equal to the sum of the depletion region and minority carrier diffusion length.[11–17]

Recently, a new approach to CQD film formation was reported. An all-inorganic CQD film was produced by displacing long, as-synthesized oleic ligands in the solid state, and replacing them instead with halide anions. This approach, known as atomic ligand passivation, led to the highest certified CQD PV efficiency reported, of 5.1%.[18] The use of halide ligands was found, using time-resolved infrared spectroscopy, to reduce the density of trap states deep within the bandgap, further contributing to good electron mobilities in these materials.

These prior reports indicated that exposure of the CQD surface to halides offers benefits in surface passivation, transport, and, ultimately, in device performance. In this manuscript we explore strategies to enhance further this passivation, rendering it more thorough and complete.

We took the view that, in the solid state treatment, steric hindrance can prevent the complete replacement of long organic ligands with halide anions. Herein we explore the use of a first halide treatment, delivered to the CQDs while they are in the solution phase, whose goal is to provide a further opportunity for halides to bind surface cations.

Our solution-phase halide treatment is depicted in **Scheme 1**. Tetrabutylammonium iodide (TBAI) salts are dissolved in oleylamine (via complexation with the amine group[19]) while heating. The resultant halide-amine complex was added to a solution of CQDs dispersed in toluene solution; here the miscibility of oleylamine with toluene is exploited. Dots were then washed using ethanol and redispersed in octane.

We used X-ray photoelectron spectrascopy (XPS) and fourier transform infrared spectroscopy (FTIR) to find conditions under which the solution-phase halide treatment had a measurable influence on composition. XPS revealed the emergence of a strong iodide peak following the solution-phase halide treatment, with a Pb:iodide ratio of 3.7:1 (Figure S1a). XPS also showed that the amount of oleic acid (OA) ligand is reduced in the halide-treated CQD solids: the Pb:OA ratio grows from 1.7:1 to 2.5:1 after the solution-phase halide treatment. FTIR spectra (Figure S2) agree well with this finding, showing the organic C-H signal between 2800-3000 cm^{-1} to be much reduced. The results, taken together, indicate that the halide partially displaces oleic acid during the solution-phase treatment.

We used absorption and emission spectra (**Figure 1**) to study further the impact of the solution-phase halide treatment on the physical properties of the CQDs. The absolute photoluminescence quantum yield, obtained via the integrating sphere method,[20]

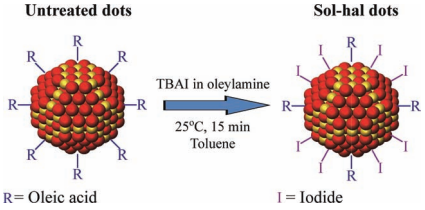

Scheme 1. The ligand exchange procedure to produce solution-phase halide treated quantum dots. TBAI was dissolved in oleylamine at 200 °C (0.6 M) under nitrogen. 0.5 mL TBAI was added to 6 mL of quantum dots in toluene (50 mg mL^{-1}) and stirred for 15 min at room temperature. Nanocrystals were precipitated via the addition of ethanol and then were redispersed in octane. The procedure was carried out in a dry nitrogen glovebox.

Dr. Z. Ning, Dr. Y. Ren,
Dr. S. Hoogland, Dr. O. Voznyy, Dr. L. Levina,
Dr. P. Stadler, Mr. X. Lan, Mr. D. Zhitomirsky,
Prof. E. H. Sargent
Department of Electrical and Computer Engineering
University of Toronto
10 King's College Road, Toronto, Ontario, M5S 3G4, Canada
E-mail: ted.sargent@utoronto.ca

DOI: 10.1002/adma.201202942

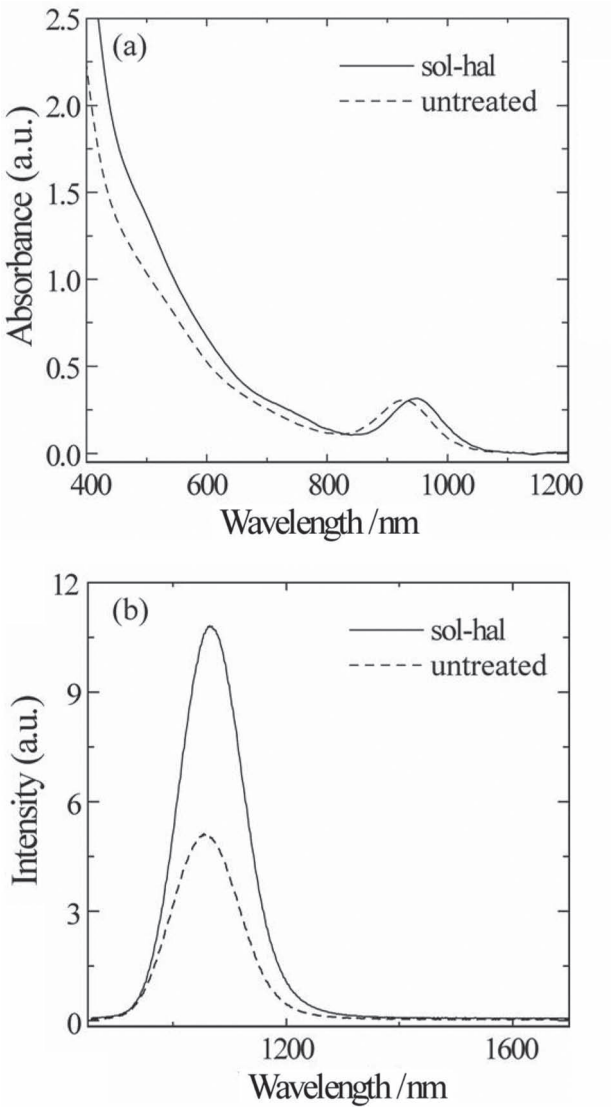

Figure 1. The absorption (a) and photoluminescence (b) spectra of untreated dots (dashed lines) and solution-phase halide treated (solid lines) dots. The absolute luminescence quantum yield of solution-phase halide treated dots is 1.7 times higher than the untreated dots. A slight redshift is observed in both absorption and photoluminescence.

of the solution-phase halide treated dots is 20%, notably higher than that of the untreated dots (12%). The increased photoluminescence suggested that, as intended, the halide treatment was helping to passivate the nanoparticles' surfaces.

Photoluminescence quantum yield provides indirect evidence of recombination centres on CQDs; we therefore sought in addition a direct measurement. The open-circuit transient decay method can be used to scan the mid-gap density of states (n) within the bandgap of a semiconductor material incorporated into a rectifying diode:

$$n = \frac{1}{Aed}\int_0^{Voc} C\,dV \quad (1)$$

where A is the device area, e is the electronic charge, d is the film thickness, and V_{oc} is the open-circuit voltage. C is the

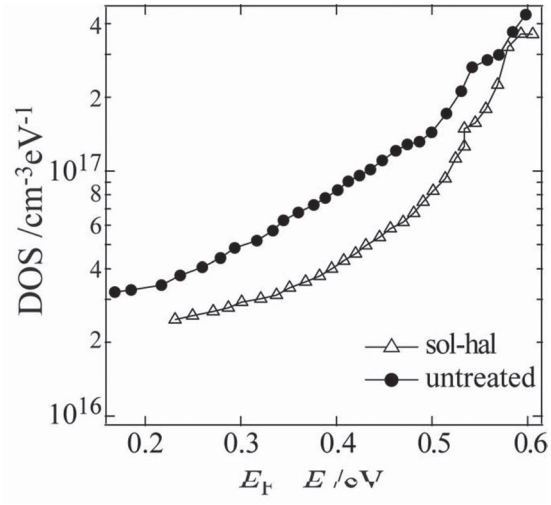

Figure 2. Density of trap states in quantum dot films made using solution-phase halide treated quantum dots (triangle) compared with untreated quantum dots (dot).

differential capacitance of the film calculated from the differential injected charge divided by the differential increase in V_{oc}. The differential injected charge is obtained by integrating the photocurrent transient decay under short circuit conditions.[21] This measurement can be applied directly to photovoltaic devices as seen below.

As seen in **Figure 2**, the density of trap states of the solution-phase halide treated dots is much lower than that of the untreated dots. This is true throughout the entire portion of the bandgap that can be visualized using transient open-circuit techniques. This range corresponds to the crucial energy range lying between the quasi-Fermi levels under 1 sun solar illumination. The result thus proves that the trap density of the solution-phase halide treated dots is considerably improved over the relevant energy range within the quantum-confined bandgap of the CQD solid.

The mobility of charge carriers inside CQD solids is a critical determinant of performance. Mobility is expected to be related to the density (close-packing) among nanoparticles, since having a close nearest-neighbour facilitates both delocalization and hopping. A further major factor is the presence of electronic trap states energetically beneath the transport band. We hypothesized that the improved density of trap states within the bandgap could also have translated into improved electron transport.

To investigate transport directly, we constructed field effect transistor test structures. The electron mobility in the films made using untreated dots was 0.03 $cm^2\ V^{-1}\ s^{-1}$ while for the solution-phase halide-treated dots it was 0.24 $cm^2\ V^{-1}\ s^{-1}$ (**Figure 3**). This order-of-magnitude improvement in mobility is explainable via the reduced trap state density independently measured via transient photovoltage. The 0.24 $cm^2\ V^{-1}\ s^{-1}$ mobility represents the highest FET mobility reported in a PbS CQD solid having a bandgap greater than 1.2 eV (corresponding to a nanoparticle size of less than 4 nm).

To explore the benefits of solution-phase halide passivation in operating solar cells, we built devices based on the p-n

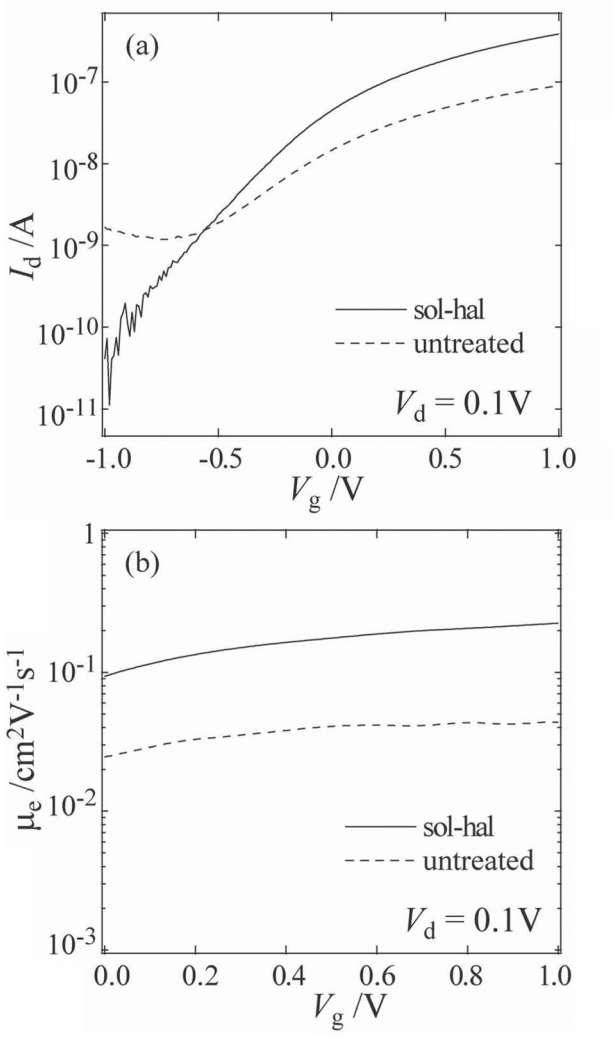

Figure 3. Field effect transistor (FET) characterization of conventional (dashed lines) and solution-phase halide-treated CQD films (solid lines). The mobility is one order of magnitude higher for the solution-phase halide-treated CQDs.

homojunction architecture.[22] The device structure and SEM cross-section are shown in **Figure 4**a. The bottom p-doped side (thickness 70 nm) is prepared by exposing the film to oxygen,[23] while device fabrication is finished entirely within a glovebox in order to prepare the thicker (230 nm) n-type halide-treated film (doping type indicated by the FET results of Figure 3). The above film thicknesses represent the optimal values we found via systematic experimental variation of the p-type and n-type layers. Overly thin p-layers caused short circuits, presumably due to incomplete coverage of the underlying electrode, while overly thick p-layer decreased fill factor. Thinner n-layers decreased the current by reducing absorbance, while excessive thickness degraded fill factor.

External quantum efficiency (EQE) spectra (Figure 4b) indicates that the solution-phase halide treatment produces the highest external quantum efficiency, the advantage particularly strong in the infrared region. The infrared response is a sensitive probe of the efficiency of charge carrier extraction from the back side of the device, since weaker absorption per unit length in this range ensures more photocarrier generation near the back of the device, far from the metallurgical junction.

A thicker depletion region, which would be produced if the doping was appreciably lower on the n-side of the junction in the solution-phase halide-treated case, could offer one explanation for improved infrared extraction. We used capacitance-voltage measurements to obtain the doping density (Figure S3) and found that, both for untreated and solution-phase halide-treated CQDs, the doping lay in the narrow range 2.0–2.3 × 10^{16} cm^{-3}. Especially since depletion depth goes as the square-root of doping density, this is a marginal impact, and we conclude that the extent of the depletion region was not materially altered by the halide treatment.

The primary reason for the improved current is therefore that recombination was reduced, and mobility increased, as established in transient photovoltage and transport measurements. This led to improved photocurrent, especially for photocarriers having to travel the longest distance to be extracted.

We conclude by summarizing the performance of each class of device, the control devices and the solution-phase halide treated devices (Figure 4c and **Table 1**). Solution-phase halide treated devices show a noticeably higher fill factor and an increased photocurrent. Improved transport enhances fill factor by lowering series resistance, and improved trap passivation increases shunt resistance by reducing recombination.

Ultimately, these improvements led to an evidently higher AM 1.5 solar power conversion efficiency of 6.6% compared to 5.6% for the untreated dots.

In summary, in this manuscript, we introduced solution-phase passivation using halide anions and proved that the approach appreciably reduced traps in PbS CQD films. This new process led to record carrier mobility for PbS CQD films having a solar-optimal bandgap, their electron mobility fully one order of magnitude higher than via prior CQD processes. Based on these better-passivated, lower-trap-density, higher-mobility, solution-phase halide treated CQD films, the highest efficiency for all-inorganic CQD solar cells was achieved. The halide-passivation strategy offers further potential to overcome the key limitations – the cleanliness of the bandgap and its impact on recombination – that, once addressed, will enable enhanced light harvesting efficiency in low-cost solution-processed solar cells.

Experimental Section

Solution halide precursor preparation: TBAI precursor preparation: TBAI was dissolved in oleylamine by heating at 200 °C for 2 hours under N_2 in Schlenk line, and then pumping for 2 hours at 100 °C. The solution was kept at 40 °C to avoid solidification. A precursor with concentration of 0.6 M was obtained by dissolving TBAI (2.21 g, 6 mmol) in oleylamine (10 mL).

CQD synthesis and solution halide treatment: Untreated PbS CQDs were synthesized according to a previously reported procedure.[13,24] For solution halide treatment, untreated dots (50 mg mL^{-1}) in toluene (6 mL) were added to TBAI precursor (0.6 mL) in a vial. The solution was stirred at room temperature for 15 minutes. Ethanol was added to precipitate the dots, and the solution was centrifuged to separate the CQDs powder from solution. The nanocrystals were finally dispersed in octane (50 mg mL^{-1}). The ligand exchanging process was carried out in

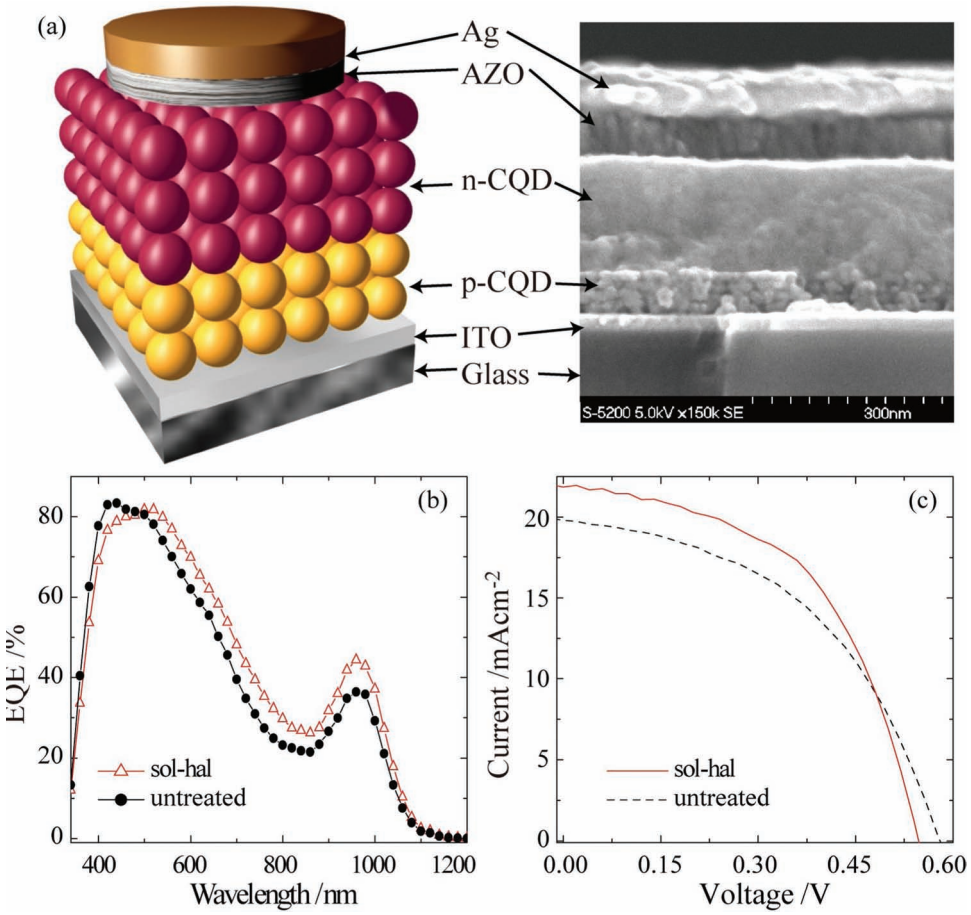

Figure 4. Solar cells employing control vs. solution-phase halide-treated CQDs. (a) The structure and cross-section scanning electron microscopy (SEM) of the device. The p-layer and n-layer can be distinguished in the SEM image. (b) The EQE spectra for the control and positive devices; a higher EQE is apparent in the infrared spectral region for the solution-phase halide treated CQDs (c) *I-V* curves of the different devices under 1 sun AM1.5 solar illumination. The photocurrent and fill factor are notably increased when solution-phase halide-treated quantum dots are employed, as seen in Table 1.

a dry nitrogen glovebox (Oxygen level below 2 ppm and moisture level below 10 ppm).

Film deposition: Layer-by-layer (LBL) spin-coating was employed to fabricate the CQD film. Deposition of the p-layer was carried out in air as follows:

1) 3 drops of PbS CQDs in octane (30 mg mL^{-1}) were deposited onto ITO-coated glass (25 mm × 25 mm) substrates and were spin-cast at 2500 RPM for 10 s;
2) Tetramethylammonium hydroxide pentahydrate (TMAOH) (0.75 mL of 10 mg mL^{-1}) methanol solution were deposited and left on the film for 10 s. This was followed by spinning at 2500 RPM for 10 s (repeat twice);
3) Methanol (0.75 mL) was dropped and spin-cast at 2500 RPM for 10 s (repeat twice). Steps 1–3 were repeated until the desired thickness of PbS CQDs films was reached (3 repeats corresponded to 70 nm of p-type material). The as-deposited p-layer samples were annealed at 50 °C in air for 12 h and then transferred into a N_2-glovebox for n layer deposition. Similar deposition protocols were employed to fabricate n-layers using TBAI treatments (9 repeats corresponded to 230 nm of n-type material).

Table 1. Device performance as a function of solution-phase treatment.

Type	Untreated Dots	Sol-Hal Dots
V_{oc}[V]	0.58	0.55
J_{sc}[mA/cm^2]	19.8	21.8
FF[%]	49	55
PCE[%]	5.6	6.6

Electrode deposition: Aluminum doped zinc oxide (AZO) (30 nm thick) was deposited at a rate of 0.2 Å s^{-1} using sputtering, followed by thermal evaporation of silver contacts (300 nm thick) at a rate of 2 Å s^{-1} with base pressure of 1×10^{-7} mbar. The deposition was carried out in Angstrom Engineering Åmod deposition system in an Innovative Technology glovebox.

FET measurements: FET fabrication began with thermal deposition of Al on glass substrates. Surface of Al layer was then electrochemically anodized to form an 8 nm thick Al_2O_3 gate dielectric.[25,26] This was followed by spin coating of PbS CQDs in N_2 glovebox, and post-treatment with 10 mg mL^{-1} TBAI methanol solution. Finally, titanium was deposited as top contacts. Carrier mobility μ was extracted from the linear transport regime, where drain current takes the form

$I_d = (WC_i\mu/L) \times (V_g - V_T - V_d/2)V_d$ with channel width $W = 2$ mm, channel length $L = 50$ μm and capacitance per unit area $C_i = 500$ nF cm^{-2}.

Supporting Information

Supporting Information is available from the Wiley Online Library or from the author.

Acknowledgements

This publication is based in part on work supported by Award KUS-11-009-21, made by King Abdullah University of Science and Technology (KAUST), by the Ontario Research Fund Research Excellence Program, and by the Natural Sciences and Engineering Research Council (NSERC) of Canada. We thank Angstrom Engineering, Inc. and Innovative Technology, Inc. for useful discussions regarding material deposition methods and control of the glovebox environment, respectively. The authors thank Xihua Wang for helpful discussions; Daniel Paz-Soldan, Ghada Koleilat, and Susanna Thon for measurement asisstance; and E. Palmiano, R. Wolowiec, and D. Kopilovic for assistance during the course of study.

Received: July 23, 2012
Published online: November 12, 2012

[1] E. H. Sargent, *Nat. Photonics* **2012**, *6*, 133.
[2] G. Konstantatos, I. Howard, A. Fischer, S. Hoogland, J. Clifford, E. Klem, L. Levina, E. H. Sargent, *Nature* **2006**, *442*, 180.
[3] A. J. Nozik, M. C. Beard, J. M. Luther, M. Law, R. J. Ellingson, J. C. Johnson, *Chem. Rev.* **2010**, *110*, 6873.
[4] D. V. Talapin, J.-S. Lee, M. V. Kovalenko, E. V. Shevchenko, *Chem. Rev.* **2010**, *110*, 389.
[5] P. V. Kamat, K. Tvrdy, D. R. Baker, J. G. Radich, *Chem. Rev.* **2010**, *110*, 6664.
[6] X. Wang, G. Koleilat, J. Tang, H. Liu, I. J. Kramer, R. Debnath, L. Brzozowski, D. A. R. Barkhouse, L. Levina, S. Hoogland, E. H. Sargent, *Nat. Photonics* **2011**, *5*, 480.
[7] O. E. Semonin, J. M. Luther, S. Choi, H.-Y. Chen, J. Gao, A. J. Nozik, M. C. Beard, *Science* **2011**, *334*, 1530.
[8] A. G. Pattantyus-Abraham, I. J. Kramer, A. R. Barkhouse, X. Wang, G. Konstantatos, R. Debnath, L. Levina, I. Raabe, M. K. Nazeeruddin, M. Grätzel, E. H. Sargent, *ACS Nano* **2010**, *4*, 3374.
[9] J. M. Luther, M. Law, Q. Song, C. L. Perkins, M. C. Beard, A. J. Nozik, *ACS Nano* **2008**, *2*, 271.
[10] J. Tang, E. H. Sargent, *Adv. Mater.* **2011**, *23*, 12.
[11] A. K. Rath, M. Bernechea, L. Martinez, G. Konstantatos, *Adv. Mater.* **2011**, *23*, 3712.
[12] H. Liu, J. Tang, I. J. Kramer, R. Debnath, G. I. Koleilat, X. Wang, A. Fisher, R. Li, L. Brzozowski, L. Levina, E. H. Sargent, *Adv. Mat.* **2011**, *23*, 3832.
[13] D. Aaron R. Barkhouse, R. Debnath, I. J. Kramer, D. Zhitomirsky, A. G. Pattantyus-Abraham, L. Levina, L. Etgar, M. Grätzel, E. H. Sargent, *Adv. Mat.* **2011**, *23*, 3134.
[14] W. Ma, S. L. Swisher, T. Ewers, J. Enge, V. E. Ferry, H. A. Atwater, A. P. Alivisatos, *ACS Nano* **2011**, *5*, 8140.
[15] A. Braga, S. Gimenez, I. Concina, A. Vomiero, I. Mora-Sero, *J. Phys. Chem. Lett.* **2011**, *2*, 454.
[16] D. F. Wang, H. G. Zhao, N. Q. Wu, M. A. El Khakani, D. L. Ma, *J. Phys. Chem. Lett.* **2010**, *1*, 1030.
[17] J. B. Gao, J. M. Luther, O. E. Semonin, R. J. Ellingson, A. J. Nozik, M. C. Beard, *Nano Lett.* **2011**, *11*, 1002.
[18] J. Tang, K. W. Kemp, S. Hoogland, K. S. Jeong, H. Liu, L. Levina, M. Furukawa, X. Wang, R. Debnath, D. Cha, K. W. Chou, A. Fischer, A. Amassian, J. B. Asbury, E. H. Sargent, *Nat. Mater.* **2011**, *10*, 765.
[19] I. Moreels, Y. Justo, B. De Geyter, K. Haustraete, J. Martins, Z. Hens, *ACS Nano* **2011**, *5*, 2004.
[20] J. C. de Mello, H. F. Wittmann, R. H. Friend, *Adv. Mater.* **1997**, *9*, 230.
[21] B. C. O'Regan, S. Scully, A. C. Mayer, E. Palomares, J. Durrant, *J. Phys. Chem. B* **2005**, *109*, 4616.
[22] J. Tang, H. Liu, D. Zhitomirsky, S. Hoogland, X. Wang, M. Furukawa, L. Levina, E. H. Sargent, *Nano Lett.* **2012**, DOI: 10.1021/nl302436r.
[23] J. Tang, L. Brzozowski, D. A. R. Barkhouse, X. Wang, R. Debnath, R. Wolowiec, E. Palmiano, L. Levina, A. G. Pattantyus-Abraham, D. Jamakosmanovic, E. H. Sargent, *ACS Nano* **2010**, *4*, 869.
[24] M. A. Hines, G. D. Scholes, *Adv. Mat.er* **2003**, *15*, 1844.
[25] M. Kaltenbrunner, P. Stadler, A. W. Hassel, N. S. Sariciftci, S. Bauer, *Adv. Mater.* **2011**, *23*, 4892.
[26] P. Stadler, A. M. Track, M. Ullah, H. Sitter, G. J. Matt, G. Koller, T. B. Singh, H. Neugebauer, N. S. Sariciftci, M. G. Ramsey, *Org. Electron.* **2010**, *11*, 207.